RSC Advances

PAPER

View Article Online
View Journal | View Issue

Cite this: *RSC Adv.*, 2023, **13**, 23158

Efficacy of modified carbon molecular sieve with iron oxides or choline chloride-based deep eutectic solvent for the separation of CO_2/CH_4

Nur Indah Fajar Mukti, [abc] Teguh Ariyanto,[ac] Wahyudi Budi Sediawan[a] and Imam Prasetyo *[ac]

It is necessary to separate CO_2 from biogas to improve its quality for the production of biomethane. Herein, an improvement in the separation of CO_2/CH_4 *via* adsorption was achieved by modifying the surface of CMS. The surface modification of CMS was performed by impregnation with metal oxide (Fe_3O_4) and N-doping (DES–[ChCl:Gly]). Subsequently, the efficacy of the surface-modified CMS was investigated. This involved CMS modification, material characterization, and performance analysis. The uptake of CO_2 by CMS–DES–[ChCl:Gly] and CMS–Fe_3O_4 was comparable; however, their performance for the separation of CO_2/CH_4 was different. Consequently, CMS–DES–[ChCl:Gly] and CMS–Fe_3O_4 exhibited *ca.* 1.6 times enhanced CO_2 uptake capacity and *ca.* 1.70 times and 1.55 times enhanced CO_2/CH_4 separation, respectively. Also, both materials exhibited similar repeatability. However, CMS–DES–[ChCl:Gly] was more difficult to regenerate than CMS–Fe_3O_4, which is due to the higher adsorption heat value of the former (59.5 kJ).

Received 2nd May 2023
Accepted 15th July 2023

DOI: 10.1039/d3ra02890a

rsc.li/rsc-advances

1 Introduction

Presently, biogas and biomethane are considered to be alternative energy sources to fossil fuels and natural gas, which are derived from renewable resources. However, the composition of biogas is generally characterized by the presence of CH_4 (50–70%) and CO_2 (30–50%),[1,2] and thus the CO_2/CH_4 gas mixture must be separated to obtain a more energy-dense product, given that biomethane is a very calorific gas. In contrast, CO_2 has no calorific value.[3] Currently, membrane separation, absorption, and cryogenic separation are accessible technologies for eliminating carbon dioxide.[4,5] However, they are expensive and consume a large amount of energy. In the case of CO_2/CH_4 separation, adsorption-based separation has been proposed due to its high purity (>98% vol), ease of operation, and high energy efficiency.[6] There is a difference in the affinities and diffusivities of CO_2 and CH_4, resulting in separation through adsorption.[7] Molecular sieves, such as metal–organic frameworks (MOFs),[8–12] silica-derived molecular sieves (ZMSs),[13–17] and carbon-derived molecular sieves (CMSs)[18–22] are frequently utilized for adsorption-based separation. Generally, carbon-derived molecular sieves are durable at low adsorption temperatures and may be synthesized using coal,[23,24] polymers,[25–27] and biomass.[18,28–30] Furthermore, it can be readily regenerated.

CMS can be modified by altering their pores (pyrolysis, partial gasification, and pore constriction) and their surfaces (functionalization and metal impregnation). Furthermore, CMS can be homogeneous regarding their pore size by tuning their pores. Nevertheless, it is quite challenging to achieve a uniform pore size. In contrast, surface modification aims to enhance the affinity of CO_2 for carbon surfaces. In addition to the uniformity of the pores in CMS, the diffusivity of molecules in their pores is also affected by their affinity with the surface of CMS. Increasing the affinity of a molecule for the surface of CMS inhibits the mobility (diffusion) of the molecule in the pores.

In CO_2/CH_4 separation with surface modification, functional groups such as nitrogen, amines, and oxygen are usually added to CMS to increase their affinity for CO_2.[31] Also, their surface can be modified by impregnating them with metal oxides. In this case, several metal oxides have been used as CO_2 adsorbents, such as MgO, CaO, Fe_3O_4, CuO and NiO. The surface modification is based on the presence of CO_2, which has an affinity for basic metal oxides, whereas CH_4 does not. As a result of these differences, CO_2 can be removed from gas mixtures by utilizing the interaction between the adsorbate and adsorbent. Thus, the presence of basicity may enhance the surface affinity of CMS for CO_2.[32] In general, the presence of metal oxides[33] and functional groups such as oxygen and nitrogen[31] is considered to increase the affinity of CMS for CO_2. CO_2 adsorption may also occur on materials with open metal oxide sites, specific functional

[a]*Department of Chemical Engineering, Faculty of Engineering, Universitas Gadjah Mada, Yogyakarta, 55281, Indonesia. E-mail: imampras@ugm.ac.id*

[b]*Department of Chemical Engineering, Faculty of Industrial Technology, Universitas Islam Indonesia, Yogyakarta, 55584, Indonesia*

[c]*Carbon Material Research Group, Department of Chemical Engineering, Universitas Gadjah Mada, Yogyakarta, 55281, Indonesia*

groups, and charge species. As a result of the higher polarizability of CO_2, higher amounts of CO_2 are adsorbed than CH_4 at ambient temperatures. Therefore, it can be separated from gas mixtures at this temperature.[34]

Recent research has focused on enhancing activated carbon *via* surface modification to increase its affinity for CO_2. Given that CO_2 is a weak Lewis acidic gas, modifying the surface of activated carbon with basic groups or reacting it with N-containing compounds can generate more active functional sites for CO_2, enhancing the affinity for CO_2. For instance, Masruroh *et al.*[21] suggested that functionalizing the surface of activated carbon with amine groups such as monoethanolamine (MEA), 2-amino-2-methyl-1-propanol (AMP), and diethanolamine (DEA) is advantageous for improving the surface chemistry, which provides a higher affinity, thereby enhancing its CO_2/CH_4 separation performance. The results indicated that CMS–MEA exhibited the best performance for the separation of CO_2 from CH_4. In the investigation by Mukti *et al.*,[22] an improved iron oxide dispersion on oxidized carbon surfaces could separate CO_2/CH_4. In this respect, Fe_3O_4 is more desirable for separating CO_2/CH_4 than Fe_2O_3. An additional study was conducted by Schott *et al.*[35] on activated mesoporous carbon (AMC), which was modified with metal oxides (CeO_2, CuO, Mn_3O_4, and NiO) to improve its CO_2/N_2 selectivity. Compared to the parent AMC, the selectivity values of the AMC modified with metal oxides were generally higher, with a 72% improvement in the selectivity of the 30% NiO-modified AMC. In addition, Shahkarami *et al.*[36] found that MgO-impregnated activated carbon improved both the CO_2 adsorption and CO_2/N_2 selectivity.

In addition, numerous studies investigated the possibility of transforming activating agents from chemical solvents to green solvents to increase the affinity of carbon for CO_2, such as adding a deep eutectic solvent (DES) to its surface. For example, a choline chloride-based DES exhibited a strong electrostatic interaction with CO_2, contributing to an increase in the affinity for it. Ariyanto *et al.*[20] investigated the possibility of modifying carbon surfaces using a choline chloride-based DES to separate CO_2/CH_4. In their study, three types of alcohol were, *i.e.*, 1-butanol (-ol), ethylene glycol (-diol), and glycerol (-triol), were combined with choline chloride to form a DES as a surface modifier. Among them, the DES containing the triol of glycerol displayed the best performance. Hussin *et al.*[37] compared the impregnation of a deep eutectic solvent (DES) from a mixture of choline hydroxide : urea and choline hydroxide : glycerol on carbon to enhance the CO_2 adsorption capacity. The highest CO_2 adsorption efficiency was observed for the DES-based activated carbon obtained using a mixture of choline hydroxide : urea at a temperature of 25 °C. The modified adsorbent still demonstrated an excellent performance after 11 adsorption cycles and desorption.

In the present study, we synthesized molecular sieves to separate CO_2/CH_4 by impregnating porous carbon surfaces with Fe_3O_4 or DES–[ChCl:Gly]. The procedure for the preparation of CMS involved an oxidation process, followed by an impregnation process using Fe_3O_4 or DES–[ChCl:Gly]. In this study, we investigated different surface modifications and the corresponding separation performance. To the best of our knowledge, this has not been reported to date. The efficacy of DES–[ChCl:Gly] and Fe_3O_4 impregnation was assessed by examining the adsorption isotherms, breakthrough analysis, repeatability performance, and regeneration of the samples. Furthermore, their surface morphology, surface properties, elemental composition, and chemical properties were evaluated using SEM-EDX mapping, FTIR, and nitrogen sorption analysis.

2 Experimental

2.1. Materials

The materials used included porous carbon with a mesh size of 20–25, ferrous(III) nitrate (Merck), H_2O_2 (Merck), choline chloride (Sigma-Aldrich), glycerol (Sigma-Aldrich), methanol (Merck), HP-nitrogen, UHP-carbon dioxide and UHP-methane from PT Aneka Gas Industri Indonesia. A biogas representative comprised of CH_4 and CO_2 (55/45 v/v) was obtained from PT Aneka Gas Industri Indonesia.

2.2. Modification of CMS

Pristine carbon with a mesh size of 20–25 was pre-treated with 10% H_2O_2 to increase its surface wettability. In the next step, pre-treated carbon was impregnated with Fe_3O_4 and DES–[ChCl:Gly]. The metal oxides (Fe_3O_4) were dispersed on pre-treated carbon using the incipient wetness method and calcined. Before impregnation, the metal salt ($Fe(NO_3)_3 \cdot 9H_2O$) was dissolved in methanol. The metal salt solution in methanol was gradually added to the carbon pores in the following stages. The use of carbon and methanol in a w/v ratio of 1 : 1 was proposed to achieve a metal oxide content of 5 wt% (Fe). In the subsequent step, the carbon was impregnated with metal salt, and then calcined at 773 K for 6 h. Information regarding the impregnation procedures can be found in the literature.[22]

DES–[ChCl:Gly] impregnation on pretreated carbon was performed in accordance with ref. 20. Choline chloride and glycerol were mixed in distilled water in a mol ratio of 0.5 : 0.5 to prepare a 5 wt% DES–[ChCl : Gly] solution. In the following step, the DES–[ChCl:Gly] solution was gradually added to the carbon pores, and then dried at 105 °C overnight. Consequently, the carbon that was impregnated with the metal oxide and DES–[ChCl:Gly] was labeled CMS–Fe_3O_4 and CMS–DES–[ChCl:Gly], respectively. The modification of CMS is schematically illustrated in Fig. 1.

2.3. Characterization of CMS

The functional groups present in the CMS materials were characterized by infrared Fourier transform analysis (FTIR) using a Nicolet Avatar 360 IR in the wavelength range of 400–4000 cm^{-1}. The morphology of CMS was examined using SEM-EDX imaging with a JEOL JSM6510 LA at 10 kV. A Quantachrome NOVA 2000 was used to record the nitrogen sorption isotherms at 77 K. The Brunauer–Emmett–Teller (BET) method was utilized to determine the surface area in the relative pressure range of 0.05 to 0.25. The total pore volume, denoted by V_t, was computed with the help of the

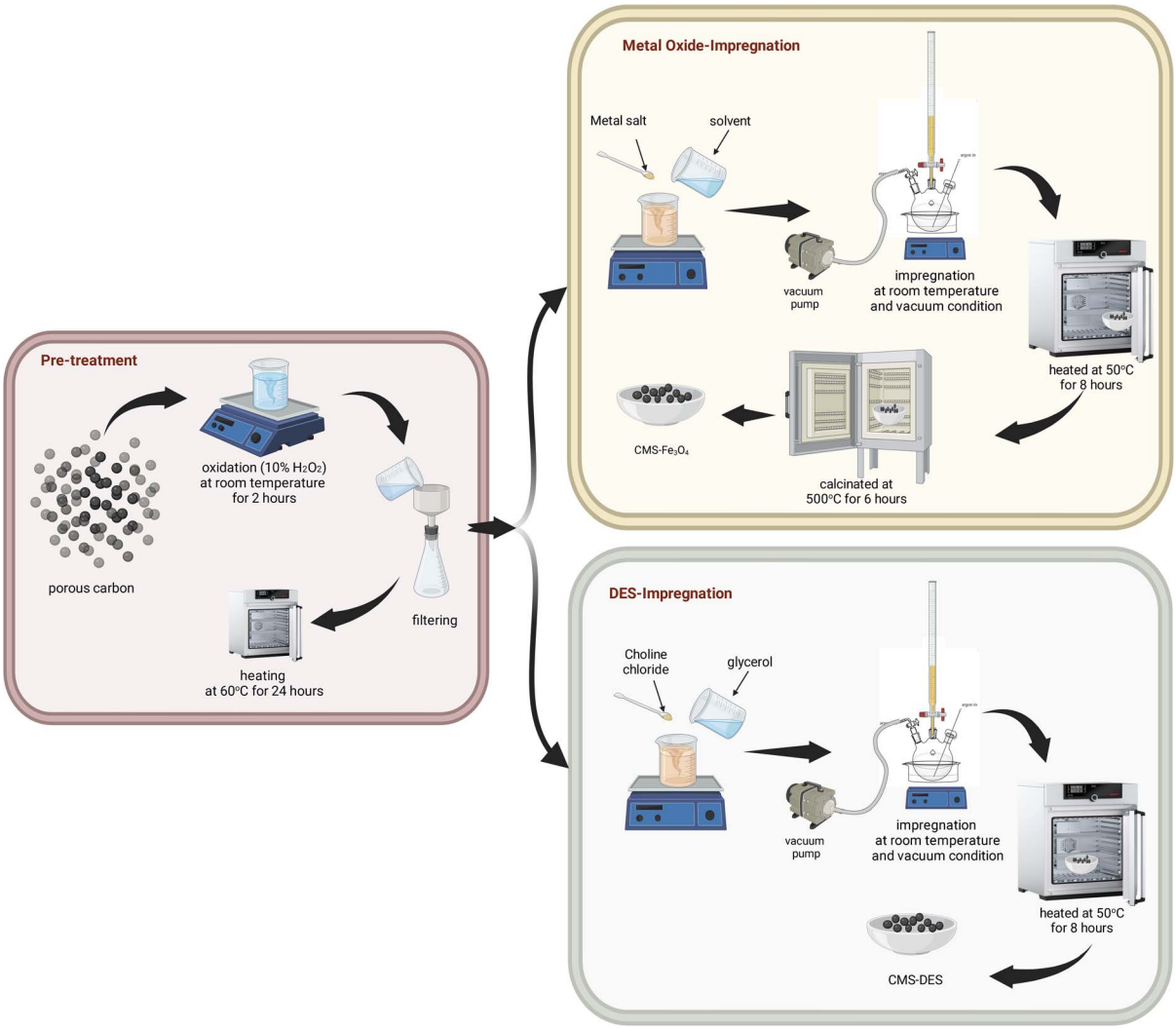

Fig. 1 Schematic of CMS modification procedure.

nitrogen sorption isotherm at a relative pressure of $P/P_0 = 0.99$. The volume of micropores (V_m) and volume of the total pore system (V_t) were calculated using the *T*-plots. The pore size distributions (PSDs) in this study were determined by density functional theory (DFT) analysis.

2.4. Measurement of adsorption isotherms

The adsorption capacity measurements for CO_2 and CH_4 were conducted at 303 K using the volumetric method. A Swagelok® VCR valve and fitting were used to assemble an ultrahigh vacuum adsorption apparatus. As a precondition for the adsorption measurements, the CMS sample was degassed at a temperature of 423 K for 6 h under vacuum. This was conducted to eliminate any remaining water and surface species. The adsorption isotherms were measured in the range of 0 to 5.0 atm and the adsorption isotherm curves were depicted using the obtained information. Detailed schematic diagrams of the adsorption isotherms and procedures for their measurements are described in the literature.[38]

2.5. Evaluation of breakthrough curves

Gas mixtures of CH_4 and CO_2 were detected using a portable biogas analyzer (Gas Board 3200 plus, Hubei Cubic Ruiyi Instrument Co., Ltd.). The CMS material was loaded in a fixed bed column ($d = 0.95$ cm and length = 30 cm), and 0.2 L min^{-1} of nitrogen gas was injected to remove CH_4, CO_2, and O_2 from the bed. The CH_4–CO_2 gas mixture entered the system at a rate of 0.05 L min^{-1} at a temperature of 303 K and pressure of 1.2 bar. After completing the separation process, the gas composition returned to its initial concentration. The detailed procedure and breakthrough system for the separation of CO_2/CH_4 are described in the literature.[20,22]

3 Results and discussion

3.1. Structural and surface characterization of CMSs

Surface morphologies and functional groups. Fig. 2(a, b and d) display the SEM images of C, CMS–DES–[ChCl:Gly], and CMS–Fe_3O_4, and Fig. 2(c and e) show the elemental mappings of

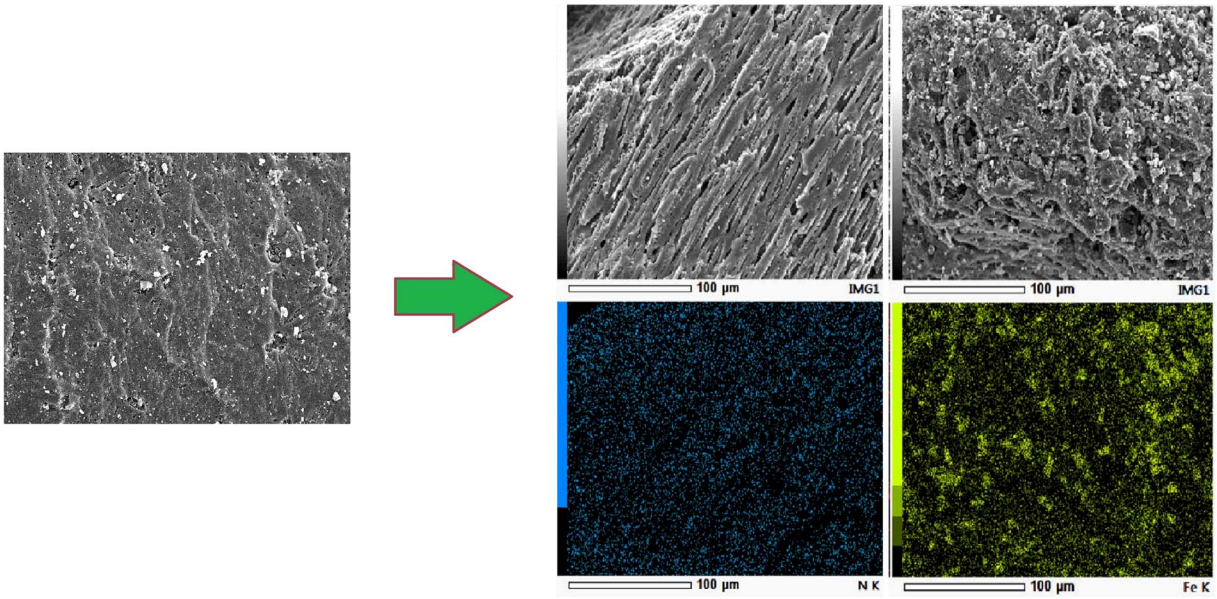

Fig. 2 SEM images and their elemental mapping of C (a), CMS–DES–[ChCl]:Gly (b and c) and CMS–Fe_3O_4 (d and e).

Table 1 The elements detected by EDX analysis on CMSs

	Element, %					
Material	C	O	N	Cl	Fe	pH_{PZC}
C	93.06	6.94	—	—	—	6.93
CMS–DES–[ChCl:Gly]	77.88	16.55	5.25	0.32	—	7.21
CMS–Fe_3O_4	83.47	10.57	—	—	5.96	7.29

CMS–DES–[ChCl:Gly] and CMS–Fe_3O_4, respectively, where differences in the surface morphology between the pristine carbon and CMSs can be observed. According to Fig. 2(a, b, and d), CMSs have more cavities than pristine carbon. It is also evident from the elemental mapping displayed in Fig. 2(c and e) that Fe_3O_4 and DES–[ChCl:Gly] were evenly distributed on the surface of the carbon. An analysis of the SEM-EDX results was performed to assess the composition of the CMSs. Table 1 provides a detailed analysis of the results.

The modification process involving iron oxide impregnation and DES–[ChCl:Gly] could alter the surface chemistry of CMS, where the addition of DES–[ChCl:Gly] and iron oxide to CMS increased its basicity. This was evidenced by the increase in the pH_{PZC} value, as shown in Table 1. The pH_{PZC} value also increased for the composite containing iron oxide and activated carbon nanoparticles.[39,40] This basicity favours CO_2 adsorption. As the basicity increased, the CO_2 affinity increased, while the CH_4 affinity decreased. In Table 1, it is also important to note that N, O, and Cl functional groups were added in the case of DES–[ChCl:Gly] impregnation. The presence of N, O, H, and Cl will increase the affinity for CO_2.

The incorporation of Fe_3O_4 and DES–[ChCl:Gly] in the porous carbon was confirmed by FTIR spectroscopy (Fig. 3). In the pristine carbon and CMSs, the peaks at 1080 cm^{-1}, 1590 cm^{-1}, and 3460 cm^{-1} are associated with the C–O groups

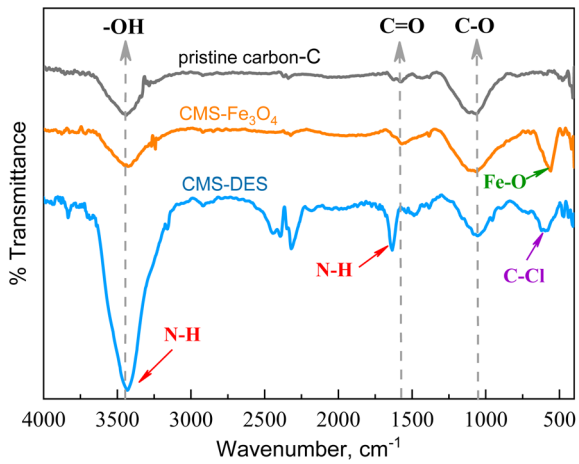

Fig. 3 FTIR spectra of C, CMS–Fe_3O_4 and CMS–DES–[ChCl]:Gly.

(stretching),[41] carboxyl groups (C=O stretching),[41,42] and hydroxyl groups (O–H stretching),[42,43] respectively. In the spectrum of CMS–DES–[ChCl:Gly], the sharp peak observed at 3440 cm^{-1} is a result of the overlap in the O–H stretch band and the N–H stretch band.[44] The FTIR spectrum of chitosan also revealed the overlap of the O–H and N–H peaks.[45] Also, DES–[ChCl:Gly] was detected on the surface of carbon based on the N–H bending peak at 1640 cm^{-1}.[20] CMS–Fe_3O_4 exhibited an additional peak at 590 cm^{-1}, indicating the presence of Fe–O bonds.[22]

Nitrogen sorption analysis. A nitrogen sorption analysis was conducted at 77 K to characterize the textural properties of pristine carbon and CMSs, and their comparison is illustrated in Fig. 4. Based on the IUPAC classification, carbon and CMS are classed as microporous materials with a type I isotherm (Fig. 4(a)). At 0.1 P/P_0, the pristine carbon exhibited a high

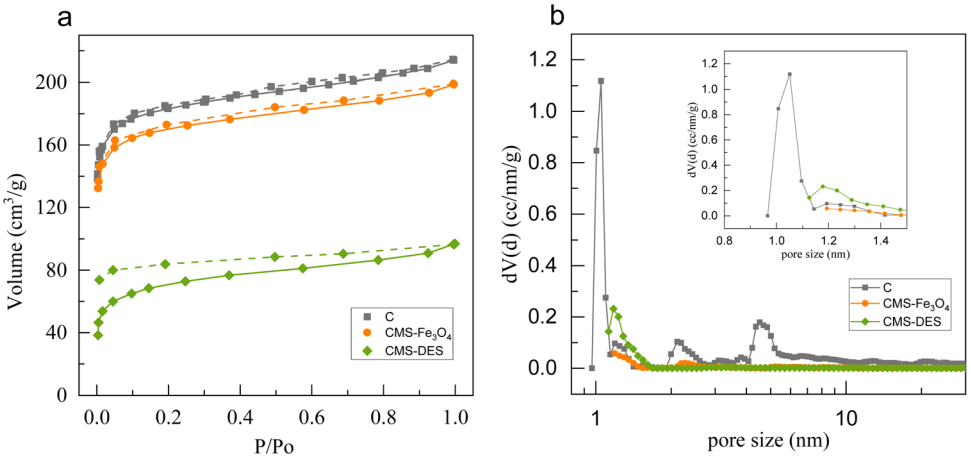

Fig. 4 Isotherms for nitrogen sorption (a) and distribution of pore sizes (b) for CMSs.

nitrogen adsorption volume (*ca.* 140 $cm^3\ g^{-1}$ STP). The volume of nitrogen adsorbed decreased significantly with CMS–DES–[ChCl:Gly], whereas it decreased modestly with CMS–Fe_3O_4. Interestingly, the adsorption–desorption isotherm curve for CMS–DES–[ChCl:Gly] is unclosed, which is probably due to the presence of ink bottle-shaped pores following impregnation.[20] Fig. 4(b) shows the results of the pore size distribution evaluated using the QSDFT model based solely on the adsorption data. The pristine carbon content was estimated to be 92 vol% in the micropore region (<2 nm), with a small tail of 4–5 nm. There was a decrease in porosity in the micropore region of CMS–DES–[ChCl:Gly] and CMS–Fe_3O_4. CMS–Fe_3O_4 exhibited a shift to <2 nm with a small tail of 2–3 nm, while CMS–DES–[ChCl:Gly] exhibited a shift to <2 nm region. A few of the small pores appeared to be blocked by DES–[ChCl:Gly] and Fe_3O_4. The pores smaller than 1 nm may become blocked completely, while that wider than 2 nm may experience a reduction in size. This can be attributed to the attachment of DES–[ChCl:Gly] and iron oxide to the carbon surface. Therefore, in the PSDs, it can be seen that the size of <2 nm was still present, while the size of >3 nm was absent.

The textural properties of CMSs are presented in Table 2. In comparison to pristine carbon, CMS–DES–[ChCl:Gly] has a lower specific surface area by approximately 64%, whereas that of CMS–Fe_3O_4 decreased by approximately 8%. The impregnation of DES–[ChCl:Gly] resulted in the blockage of the pores and the collapse of the pore walls.[20,46,47] However, regardless of their surface area or pore volume, all the materials are microporous.

Table 2 Textural properties of CMSs based on nitrogen sorption

Material	S_{BET}, $m^2\ g^{-1}$	% S_{mic}	V, $cm^3\ g^{-1}$	D_{avg}, nm
C	708	92.0	0.33	1.88
CMS–Fe_3O_4	649	92.9	0.31	1.90
CMS–DES–[ChCl:Gly]	258	86.8	0.15	2.33

3.2. Carbon dioxide and methane adsorption isotherms

As shown in Fig. 5(a and b), CO_2 and CH_4 adsorption isotherm curves were measured at 30 °C. As shown in Fig. 5(a and b), the CO_2 uptake significantly exceeded CH_4 uptake. Similar results were obtained in a previous study.[20,22] Moreover, the impregnation of Fe_3O_4 and DES–[ChCl:Gly] increased the CO_2 uptake, while reducing CH_4 uptake. In Fe_3O_4 and DES–[ChCl:Gly], the active sites are more favourable for the adsorption of CO_2, resulting in an increase in CO_2 capacity. In contrast, the carbon impregnated with Fe_3O_4 and DES–[ChCl:Gly] reduced the affinity for CH_4. Thus, the selectivity for CO_2/CH_4 was enhanced, resulting in the better removal of CO_2 from CO_2–CH_4 mixed gases. The CO_2 uptake by pristine carbon was 1.7 mol kg^{-1} at 1 atm, whereas that by CMS–Fe_3O_4 and CMS–DES–[ChCl:Gly] was 2.4 and 2.5 mol kg^{-1}, respectively. This drastically improved the CO_2 uptake, which can be attributed to factors, *i.e.*, CO_2 binding Fe_3O_4 or DES–[ChCl:Gly] functional groups in CMS and well-dispersed Fe_3O_4 and DES–[ChCl:Gly] throughout the porous carbon. Meanwhile, the uptake of pristine carbon, CMS–Fe_3O_4, and CMS–DES–[ChCl:Gly] for CH_4 was 1.1 mol kg^{-1}, 0.75 mol kg^{-1}, and 0.76 mol kg^{-1}, respectively.

The equilibrium parameters were determined using the Toth adsorption model (eqn (1)).

$$C_\mu = C_{\mu s}\frac{bP}{\left[1+(bP)^t\right]^{1/t}} \quad (1)$$

where C_μ is the uptake capacity, $C_{\mu s}$ is the maximum uptake capacity, and b and t are the equilibrium constants. Table 3 presents the parameters of the Toth model for CO_2 and CH_4 adsorption in CMSs. Based on the b value (adsorption affinity), it is clear that CO_2 is more favorably adsorbed on the CMSs than CH_4. Further, based on the b value, it can be concluded that the modified CMS exhibited an increased affinity for CO_2. In contrast, the affinity of CH_4 decreased. As shown in Table 3, the b values of CO_2 for pristine carbon, CMS–Fe_3O_4, and CMS–DES–[ChCl:Gly] are 1.53, 2.10, and 3.99, respectively.

Subsequently, it was possible to predict the simultaneous adsorption of CO_2 and CH_4 on CMSs using the equilibrium

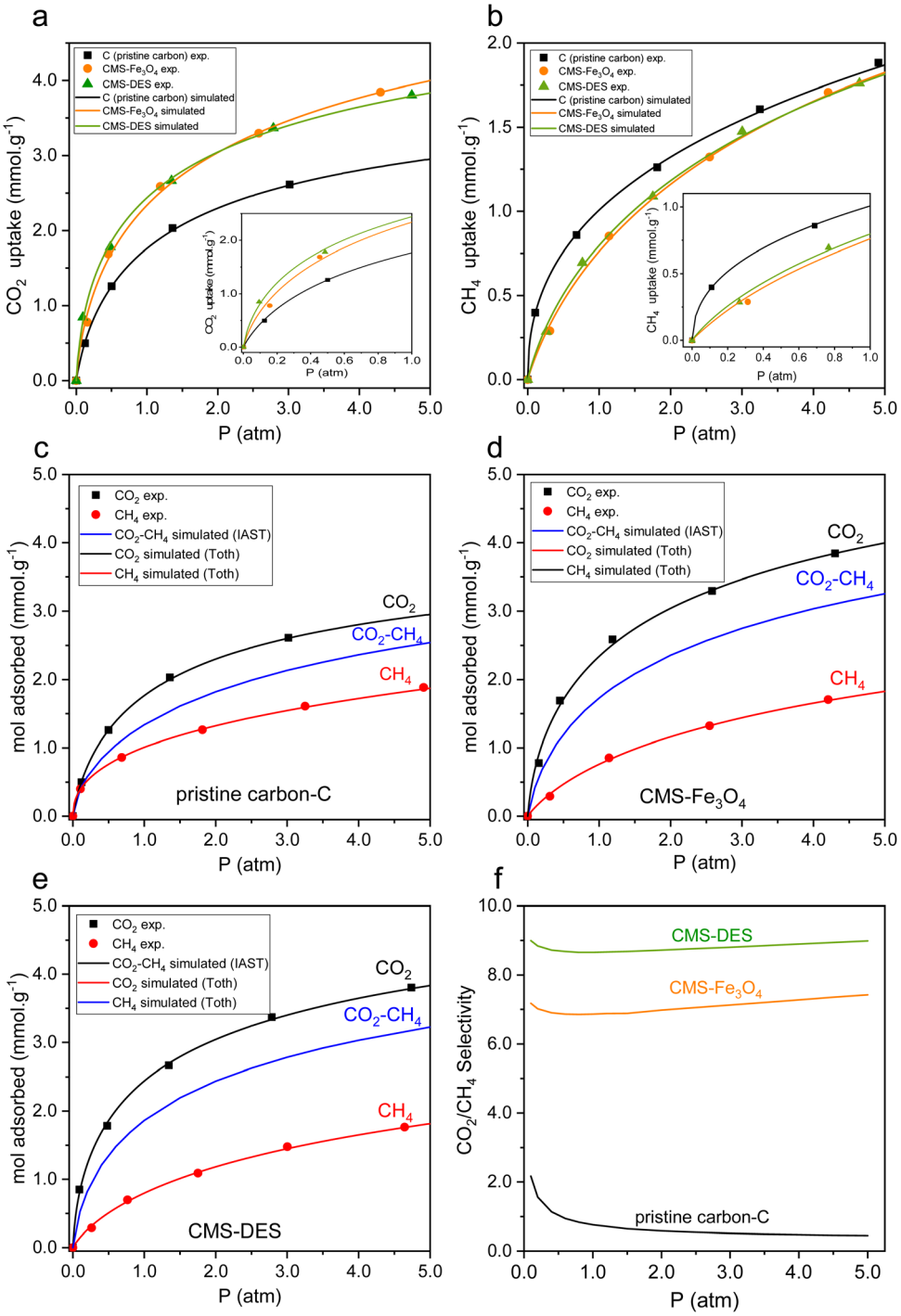

Fig. 5 Isotherm adsorption of CO_2 (a) and CH_4 (b) on pristine carbon–C, CMS–Fe_3O_4 and CMS–DES–[ChCl]:Gly, adsorption isotherm of CO_2 and CH_4 on pristine carbon–C (c), CMS–Fe_3O_4 (d) and CMS–DES–[ChCl]:Gly (e) (isotherm data fitted with the Toth equilibrium model and IAST model used in simulative adsorption of CO_2–CH_4 (55 : 45) on pristine carbon–C, CMS–Fe_3O_4 and CMS–DES–[ChCl]:Gly), sorption selectivity of CO_2/CH_4 at a temperature of 303 K (f).

adsorption of the single components of CO_2 and CH_4 on CMSs (written as CO_2–CH_4). The ideal adsorption solution theory (IAST) approximates the equilibrium equations for multicomponent systems by applying eqn (3) and (4), where the total amount absorbed can be determined. Fig. 5(c–e) present the calculation results for CO_2–CH_4 multicomponent adsorption based on the IAST model. The composition of the CO_2–CH_4 adsorption is 45% : 55%. Based on the IAST equation for CO_2–CH_4 adsorption, the maximum adsorption capacity was smaller than that for single CO_2 components. The results indicate competition for the interaction between CH_4 and CO_2 on CMSs. CO_2 is more readily adsorbable than CH_4, depending on the

Table 3 Equilibrium parameters obtained from the fitting isotherm data using the Toth model

Sample	Adsorbate	$C_{\mu s}$, (mmol g^{-1})	b (atm)	t
C	CO_2	4.47	1.53	0.62
	CH_4	3.96	0.81	0.08
	CO_2–CH_4	9.09	1.61	0.32
CMS–Fe_3O_4	CO_2	7.70	2.10	0.45
	CH_4	4.71	0.33	0.59
	CO_2–CH_4	7.13	1.13	0.47
CMS–DES–[ChCl:Gly]	CO_2	6.73	3.99	0.43
	CH_4	5.09	0.41	0.51
	CO_2–CH_4	6.51	2.02	0.43

b values of the single components in each CMS. This is also evident from the CO_2–CH_4 curve, which tends to be more closely related to CO_2.

$$C_{\mu}^{0} = f^{0}(P_{j}^{0}) \quad (2)$$

$$\frac{1}{C_{\mu T}} = \sum_{j=1}^{N} \frac{x_j}{C_{\mu j}^{0}} \quad (3)$$

The separation of CO_2/CH_4 depends heavily on the selectivity of CO_2/CH_4. Fig. 5(f) illustrates the selectivity of CO_2/CH_4. In accordance with the studies in the literature, the selectivity of pristine carbon decreased with an increase in pressure, as evidenced by the data.[20,48] CO_2/CH_4 had a selectivity of *ca.* 2.3–0.5 on the pristine carbon in the pressure range studied. Compared to pristine carbon, CMS DES–[ChCl:Gly] and CMS–Fe_3O_4 exhibited improved selectivity for CO_2/CH_4. The CO_2/CH_4 selectivity increased by 3.3 times on CMS–Fe_3O_4, while that on CMS–DES–[ChCl:Gly] increased by 3.9 times. CMS–DES–[ChCl:Gly] provides almost as much CO_2 uptake as CMS–Fe_3O_4 despite its lower surface area. Additionally, CMS–DES–[ChCl:Gly] also provided higher CO_2/CH_4 selectivity. In addition to surface area, it appears that the affinity for the active site (DES–[ChCl:Gly] or Fe_3O_4) influenced the CO_2 uptake. A more favorable affinity is the basis for improving the separation of CO_2/CH_4, given that it will inhibit CO_2 diffusion in the pores, but not CH_4 diffusion. Thus, as the diffusivity ratio increases, the separation of CO_2/CH_4 will be improved.

Adsorption studies on gases consider the heat of adsorption (ΔH_{ads}) as a significant variable. It explains how adsorbents interact with their adsorbates. Employing the Van't Hoff equation (eqn (4)), it is possible to determine the heat of adsorption (ΔH_{ads}) of CO_2 and CH_4 on pristine carbon and both CMSs. The heat of adsorption was calculated in Henry's region, provided at a zero-coverage limit.

$$\frac{\Delta H}{RT^2} = -\left(\frac{\partial(\ln K)}{\partial T}\right)_{C_{\mu}} \quad (4)$$

where ΔH_{ads} is the heat of adsorption (J mol^{-1}), K is the Henry constant (dimensionless), T is the temperature (K), and R is the ideal gas constant (J (mol K)$^{-1}$). A comparison of the CO_2 and CH_4 heat adsorption on pristine carbon, CMS–DES–[ChCl:Gly], and CMS–Fe_3O_4 is shown in Table 4. The results show a lower CO_2 adsorption energy in pristine carbon than in CMS–DES–[ChCl:Gly] and CMS–Fe_3O_4. In terms of heat of adsorption, the mechanism on pristine carbon and CMS–Fe_3O_4 is physisorption, while that on CMS–DES–[ChCl:Gly] is chemisorption. Hence, the CO_2 interactions with CMS–DES–[ChCl:Gly] are stronger than that between the pristine carbon and CMS–Fe_3O_4. This may be attributed to the fact that electrostatic interactions are responsible for the strong interactions between CMS–DES–[ChCl:Gly] and CO_2. The interactions that may occur include those involving oxygen in CO_2 with N^+ in choline, oxygen in CO_2 with H bonds from glycerol, and carbon in CO_2 with Cl^-. The presence of *n*-functionalization on carbon has also been shown to interact

Table 4 Heat of adsorption and Henry constants for CH_4 and CO_2 in CMSs

Adsorbate	Material	ΔH_{ads} (kJ mol^{-1})	T (K)	Henry constant, K_p[a]	Henry constant, K[b]
CO_2	C	10.9	303	3.4×10^{-3}	259
			313	8.4×10^{-4}	65
			323	1.9×10^{-4}	16
	CMS–Fe_3O_4	16.4	303	3.7×10^{-3}	283
			313	1.8×10^{-3}	140
			323	6.5×10^{-4}	52
	CMS–DES–[ChCl:Gly]	59.5	303	5.2×10^{-3}	394
			313	3.8×10^{-3}	293
			323	2.1×10^{-3}	172
CH_4	C	9.8	303	8.0×10^{-4}	60
			313	4.1×10^{-4}	33
			323	3.3×10^{-4}	29
	CMS–Fe_3O_4	10.6	303	9.5×10^{-4}	72
			313	7.9×10^{-4}	62
			323	6.1×10^{-4}	49
	CMS–DES–[ChCl:Gly]	10.3	303	7.7×10^{-4}	58
			313	6.8×10^{-4}	53
			323	5.9×10^{-4}	48

[a] gmol (g atm)$^{-1}$. [b] Dimensionless, $K = (K_p \rho_p RT)/(1 - \varepsilon)$.

Table 5 The heat of adsorption and amount of CH_4 and CO_2 adsorbed in other CMSs

Adsorbate	Material	SSA_{BET}, ($m^2\ g^{-1}$)	Mol adsorbed ($mmol\ g^{-1}$) (1 atm, 303 K)	ΔH_{ads} ($kJ\ mol^{-1}$)	Ref.
CO_2	C	708	1.85	10.9	This study
	CMS–Fe_3O_4	649	2.94	16.4	This study
	CMS–DES–[ChCl:Gly]	258	2.85	59.5	This study
	AC–Fe_2O_3	212	1.10	33.2	50
	AC–Co_3O_4	185	1.60	28.1	50
	Porous carbon–La_2O_3	715	1.47	33.4	51
	S-doped microporous carbon	729	2.46	22.0	52
	N-doped microporous carbon	614	4.04	59.3	31
	AC–MgO	615	2.19	—	36
CH_4	C	708	1.08	9.8	This study
	CMS–Fe_3O_4	649	0.85	10.6	This study
	CMS–DES–[ChCl:Gly]	258	0.64	10.3	This study
	AC–Fe_2O_3	212	0.30	20.2	50
	AC–Co_3O_4	185	0.40	22.0	50

strongly with CO_2 in other studies.[49] Table 5 provides a comparison of the adsorption heat values from various sources.

3.3. CO_2/CH_4 separation: a breakthrough curve analysis

The performance of the materials in separating CO_2/CH_4 was evaluated through breakthrough analysis. Fig. 6(a) depicts the CO_2 breakthrough curves for pristine carbon and CMSs. The breakthrough curves demonstrate the ratio of the outlet concentration at a given time (C_t) to the initial inlet concentration (C_0) over time. It is evident from the data that the CO_2 breakthrough time for CMS–DES–[ChCl:Gly] and CMS–Fe_3O_4 increased compared to pristine carbon. CMSs exhibited an increase in breakthrough time by 40% compared to the pristine carbon. Due to this strong interaction between CO_2 and CMSs, the CO_2 diffusion is slower. Both CMS–DES–[ChCl:Gly] and CMS–Fe_3O_4 showed similar breakthrough times. Interestingly, CMS–Fe_3O_4 had a steeper breakthrough curve than CMS–DES–[ChCl:Gly]. This suggests that CMS–DES–[ChCl:Gly] has a stronger interaction with CO_2 than CMS–Fe_3O_4. Furthermore, other studies suggest that nitrogen-doped carbon exhibits slow adsorption kinetics.[33] In contrast, studies on pristine carbon and CMS–Fe_3O_4 indicated that mass transfer occurs instantaneously.[20,22]

During the separation of CO_2/CH_4, the ability to regenerate the absorbent is an imperative factor. Fig. 6(b) illustrates a regeneration graph for pristine carbon and CMSs. The data indicate that the regeneration time of CMS–DES–[ChCl:Gly] is longer than that of CMS–Fe_3O_4 and pristine carbon. Therefore, CMS–DES–[ChCl:Gly] will be more difficult to regenerate due to its strong interaction with CO_2. Furthermore, this conclusion is supported by the results of the adsorption heat value of CMS–DES–[ChCl:Gly], which is quite high (59.5 kJ), as explained in Section 3.2.

Fig. 7 depicts the CO_2 and CH_4 breakthrough curves for the different CMS materials. Initially, neither CH_4 nor CO_2 gas was present, as shown in Fig. 6. CH_4 with a purity of higher than 98% appeared after 200 s. This was followed by CO_2 until the concentration of CO_2 in the outlet equalled the concentration in the inlet.

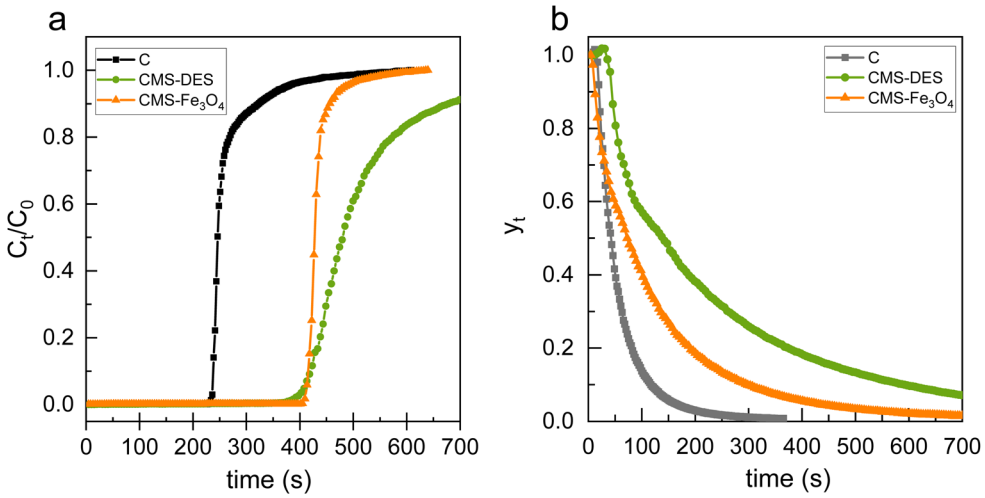

Fig. 6 CO_2 breakthrough curves of mixed gas CO_2/CH_4 for CMS (a). Desorption curves for CMS (b) at a temperature of 303 K and atmospheric pressure.

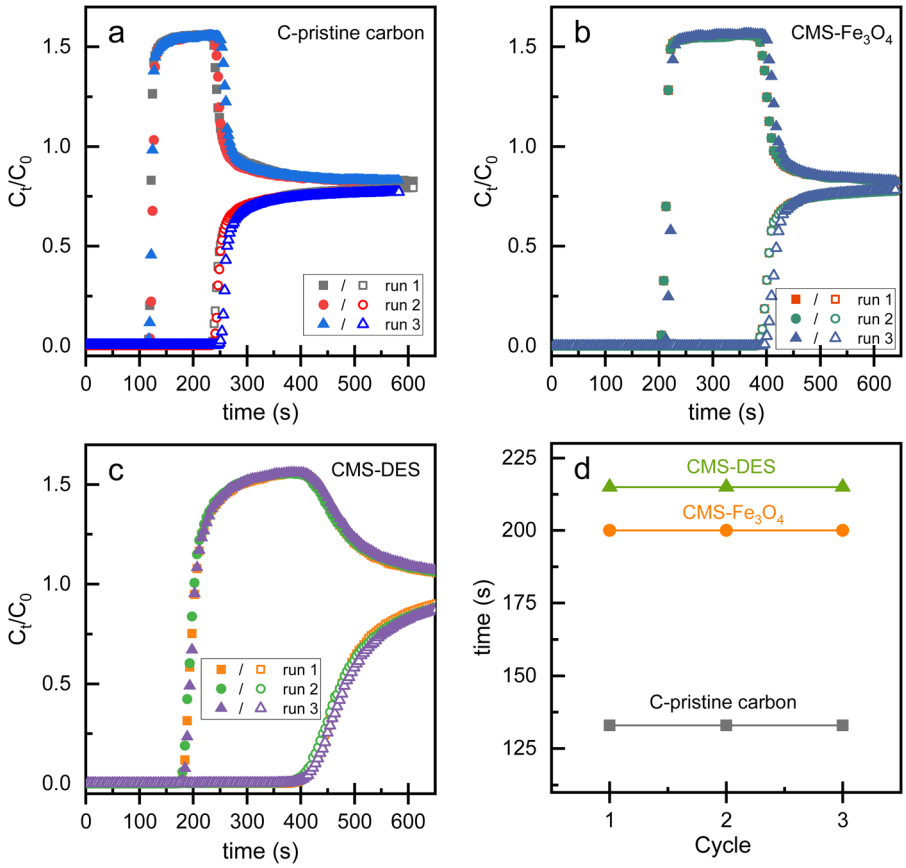

Fig. 7 Breakthrough curves of mixed gas CO_2/CH_4 for pristine carbon (a), CMS–Fe_3O_4 (b), CMS–DES–[ChCl]:Gly (c),[20] and repeatability of CO_2/CH_4 separation of CMSs (d).

Each material had a similar CH_4 breakthrough time, but a different CO_2 breakthrough time. The CMS surface and gas molecules may interact strongly, causing a delay in CO_2 flow at the outlet. Consequently, CO_2 gas diffused more slowly within the bed. Furthermore, the difference between the CH_4 signal and CO_2 signal appears to be larger, indicating that CH_4 and CO_2 were separated more effectively.

According to Fig. 7(a), the CO_2–CH_4 breakthrough time difference for pristine carbon is 130 s. CMS–Fe_3O_4 exhibited an approximately 1.5-fold increase in CO_2–CH_4 breakthrough time compared to the pristine carbon (see Fig. 7(b)). Meanwhile, CMS–DES–[ChCl:Gly] experienced a 1.7-fold increase (Fig. 7(c)). In the repeatability study, the sequence of CO_2/CH_4 separation was cycled and the bed was regenerated once it was full of CO_2. Interestingly, CMS–DES–[ChCl:Gly] and CMS–Fe_3O_4 maintained their breakthrough time in the three cycles. These materials performed similarly to the pristine carbon but had a much higher capacity for uptake. The cycling tests indicate that CMS–DES–[ChCl:Gly] and CMS–Fe_3O_4 can be repeatably used in terms of separation. Thus, it is evident that CMS–DES–[ChCl:Gly] has a wider CO_2–CH_4 breakthrough time difference and reasonable repeatability. Nevertheless, it requires a longer period for regeneration. Meanwhile, CMS–Fe_3O_4 has a shorter CO_2–CH_4 breakthrough time than CMS–DES–[ChCl:Gly]. Despite this, it is repeatable and regenerates quickly.

4 Conclusions

A feasibility study was conducted regarding the modification of CMS by impregnating DES–[ChCl:Gly] and Fe_3O_4 in the surface of porous carbon for CO_2/CH_4 separation. Several aspects of CO_2/CH_4 separation were evaluated, including CO_2 breakthrough time, CO_2–CH_4 breakthrough time difference, regeneration capability, and repetition cycle. Additionally, the uptake of CO_2 and CH_4 was examined. The CO_2–CH_4 breakthrough time difference for CMS–DES–[ChCl:Gly] was higher than that for CMS–Fe_3O_4. Consequently, CMS–DES–[ChCl:Gly] and CMS–Fe_3O_4 exhibited an enhanced CO_2 uptake capacity by *ca.* 60% at 30 °C and 1 atm, while enhancing the separation of CO_2/CH_4 by *ca.* 69% and 54%, respectively. The adsorption energy of CO_2 in CMS–DES–[ChCl:Gly] (59.5 kJ) was higher than that of CMS–Fe_3O_4 (16.4 kJ), and thus a longer regeneration time was required. According to the cycling tests, CMS–DES–[ChCl:Gly] and CMS–Fe_3O_4 could be repeatably used. Thus, CMS–Fe_3O_4 is more favourable for CO_2/CH_4 separation than CMS–DES–[ChCl:Gly]. This is due to its repeatability and ability to be regenerated quickly.

Author contributions

Nur Indah Fajar Mukti: conceptualization, investigation, methodology, formal analysis, funding acquisition, writing-

original draft. Teguh Ariyanto: supervision, funding acquisition, writing-review and editing. Wahyudi Budi Sediawan: supervision, writing-review and editing. Imam Prasetyo: conceptualization, supervision, funding acquisition, writing-review and editing.

Conflicts of interest

There are no conflicts to declare.

Acknowledgements

This research was supported by World Class Research Grant, Ministry of Education, Culture, Research, and Technology of the Republic of Indonesia, grant number 1786/UN1/DITLIT/DitLit/PT.01.03/2022. N. I. F. M. acknowledges doctoral scholarship (Beasiswa Unggulan Dosen Indonesia) through Indonesia Endowment Fund for Education.

References

1 I. U. Khan, M. H. D. Othman, H. Hashim, T. Matsuura, A. F. Ismail, M. Rezaei-DashtArzhandi and I. W. Azelee, *Energy Convers. Manage.*, 2017, **150**, 277–294.
2 R. Zhang, *Biogas and Fuel Cell Workshop*, 2012, pp. 1–8.
3 M. T. Kallo and M. J. Lennox, *Langmuir*, 2020, **36**, 13591–13600.
4 O. W. Awe, Y. Zhao, A. Nzihou, D. P. Minh and N. Lyczko, *Waste Biomass Valorization*, 2017, **8**, 267–283.
5 X. Y. Chen, H. Vinh-Thang, A. A. Ramirez, D. Rodrigue and S. Kaliaguine, *RSC Adv.*, 2015, **5**, 24399–24448.
6 I. Durán, N. Álvarez-Gutiérrez, F. Rubiera and C. Pevida, *Chem. Eng. J.*, 2018, **353**, 197–207.
7 I. Prasetyo, R. Rochmadi and E. Wahyono, *Reaktor*, 2010, **13**, 24–30.
8 W. Lou, J. Yang, L. Li and J. Li, *J. Solid State Chem.*, 2014, **213**, 224–228.
9 D. Britt, H. Furukawa, B. Wang, T. G. Glover and O. M. Yaghi, *Proc. Natl. Acad. Sci. U. S. A.*, 2009, **106**, 20637–20640.
10 W. L. Queen, M. R. Hudson, E. D. Bloch, J. A. Mason, M. I. Gonzalez, J. S. Lee, D. Gygi, J. D. Howe, K. Lee, T. A. Darwish, M. James, V. K. Peterson, S. J. Teat, B. Smit, J. B. Neaton, J. R. Long and C. M. Brown, *Chem. Sci.*, 2014, **5**, 4569–4581.
11 Z. Li, P. Liu, C. Ou and X. Dong, *ACS Sustainable Chem. Eng.*, 2020, **8**, 15378–15404.
12 A. Guo, Y. Ban, K. Yang and W. Yang, *J. Membr. Sci.*, 2018, **562**, 76–84.
13 N. K. Jensen, T. E. Rufford, G. Watson, D. K. Zhang, K. I. Chan and E. F. May, *J. Chem. Eng. Data*, 2012, **57**, 106–113.
14 M. Younas, M. Sohail, L. L. Kong, M. J. K. Bashir and S. Sethupathi, *Int. J. Environ. Sci. Technol.*, 2016, **13**, 1839–1860.
15 A. I. Sarker, A. Aroonwilas and A. Veawab, *Energy Procedia*, 2017, **114**, 2450–2459.
16 R. Chanajaree, T. Chokbunpiam, J. Kärger, S. Hannongbua and S. Fritzsche, *Microporous Mesoporous Mater.*, 2019, **274**, 266–276.
17 W. Li, K. Goh, C. Y. Chuah and T. H. Bae, *J. Membr. Sci.*, 2019, **588**, 117220.
18 I. Prasetyo, N. I. F. Mukti, R. B. Cahyono, A. Prasetya and T. Ariyanto, *Waste Biomass Valorization*, 2020, **11**, 5599–5606.
19 I. Prasetyo and D. D. Do, *Chem. Eng. Sci.*, 1998, **53**, 3459–3467.
20 T. Ariyanto, K. Masruroh, G. Y. S. Pambayun, N. I. F. Mukti, R. B. Cahyono, A. Prasetya and I. Prasetyo, *ACS Omega*, 2021, **6**, 19194–19201.
21 K. Masruroh, R. B. Cahyono, I. Prasetyo and T. Ariyanto, *Int. J. Renewable Energy Dev.*, 2021, **10**, 249–255.
22 N. I. F. Mukti, T. Ariyanto, W. B. Sediawan and I. Prasetyo, *RSC Adv.*, 2021, **11**, 36782–36791.
23 Z. Yang, D. Wang, Z. Meng and Y. Li, *Sep. Purif. Technol.*, 2019, **218**, 130–137.
24 H. Teng, J. A. Ho, Y. F. Hsu and C. T. Hsieh, *Ind. Eng. Chem. Res.*, 1996, **35**, 4043–4049.
25 I. Prasetyo, R. Rochmadi, E. Wahyono and T. Ariyanto, *Eng. J.*, 2017, **21**, 83–94.
26 S. J. Kim, Y. Kwon, D. Kim, H. Park, Y. H. Cho, S. E. Nam and Y. I. Park, *Membranes*, 2021, **11**, 1–34.
27 C. P. Hu, C. K. Polintan, L. L. Tayo, S. C. Chou, H. A. Tsai, W. S. Hung, C. C. Hu, K. R. Lee and J. Y. Lai, *Carbon*, 2019, **143**, 343–351.
28 N. Álvarez-Gutiérrez, M. v Gil, F. Rubiera and C. Pevida, *Fuel Process. Technol.*, 2016, **142**, 361–369.
29 S. Sethupathi, M. J. Bashir, Z. A. Akbar and A. R. Mohamed, *Waste Manage. Res.*, 2015, **33**, 303–312.
30 H. Wei, J. Chen, N. Fu, H. Chen, H. Lin and S. Han, *Electrochim. Acta*, 2018, **266**, 161–169.
31 Y. Zhao, X. Liu, K. X. Yao, L. Zhao and Y. Han, *Chem. Mater.*, 2012, **24**, 4725–4734.
32 W. N. R. W. Isahak, Z. A. C. Ramli, M. W. Ismail, K. Ismail, R. M. Yusop, M. W. M. Hisham and M. A. Yarmo, *J. CO2 Util.*, 2013, **2**, 8–15.
33 B. Petrovic, M. Gorbounov and S. M. Soltani, *Microporous Mesoporous Mater.*, 2021, **312**, 110751.
34 D. Saha and M. J. Kienbaum, *Microporous Mesoporous Mater.*, 2019, **287**, 29–55.
35 J. A. Schott, Z. Wu, S. Dai, M. Li, K. Huang and J. A. Schott, *Microporous Mesoporous Mater.*, 2017, **249**, 34–41.
36 S. Shahkarami, A. K. Dalai and J. Soltan, *Ind. Eng. Chem. Res.*, 2016, **55**, 5955–5964.
37 F. Hussin, M. K. Aroua and R. Yusoff, *J. Environ. Chem. Eng.*, 2021, **9**(4), 105333.
38 I. Prasetyo, N. I. F. Mukti, M. Fahrurrozi and T. Ariyanto, *ASEAN J. Chem. Eng.*, 2018, **18**, 09–16.
39 M. Jain, M. Yadav, T. Kohout, M. Lahtinen, V. K. Garg and M. Sillanpää, *Water Resour. Ind.*, 2018, **20**, 54–74.
40 B. Buhani, S. Suharso, F. Luziana, M. Rilyanti and S. Sumadi, *Desalin. Water Treat.*, 2019, **171**, 281–293.
41 W. Yang, Z. Du, Z. Ma, G. Wang, H. Bai and G. Shao, *RSC Adv.*, 2016, **6**, 3942–3950.

42 B. Lesiak, N. Rangam, P. Jiricek, I. Gordeev, J. Tóth, L. Kövér, M. Mohai and P. Borowicz, *Front. Chem.*, 2019, **7**, 1–16.
43 F. Larasati, Y. Kusumastuti, A. Mindaryani, R. Rochmadi and M. Handayani, *ASEAN J. Chem. Eng.*, 2022, **22**, 82–92.
44 M. M. Zainol, M. N. F. Roslan, M. Asmadi and N. A. S. Amin, *ASEAN J. Chem. Eng.*, 2021, **21**, 1–10.
45 A. Ayub, Z. A. Raza, M. I. Majeed, M. R. Tariq and A. Irfan, *Int. J. Biol. Macromol.*, 2020, **163**, 603–617.
46 S. H. Khalil, M. K. Aroua and W. M. A. W. Daud, *Chem. Eng. J.*, 2012, **183**, 15–20.
47 B. G. H. Briton, L. Duclaux, Y. Richardson, K. B. Yao, L. Reinert and Y. Soneda, *Appl. Water Sci.*, 2019, **9**, 1–14.
48 W. Liang, Z. Liu, J. Peng, X. Zhou, X. Wang and Z. Li, *Energy Fuels*, 2019, **33**, 493–502.
49 D. Saha, S. E. van Bramer, G. Orkoulas, H. C. Ho, J. Chen and D. K. Henley, *Carbon*, 2017, **121**, 257–266.
50 Ã. Kirbiyikkurukavak, B. Z. Buÿükbekar and M. Ersöz, *Turk. J. Chem.*, 2021, **45**, 914–926.
51 M. Jonnalagadda, R. Anjum, H. Burri and S. Mutyala, *J. Chem. Res.*, 2021, **45**, 194–200.
52 Y. Xia, Y. Zhu and Y. Tang, *Carbon*, 2012, **50**, 5543–5553.